Nuclear Magnetic Resonance Characterization of the Jun Leucine Zipper Domain: Unusual Properties of Coiled-Coil Interfacial Polar Residues†

F. Keith Junius,‡ Joel P. Mackay,§ William A. Bubb,‡ Sacha A. Jensen,‡ Anthony S. Weiss,‡ and Glenn F. King*,‡

Department of Biochemistry, University of Sydney, Sydney NSW 2006, Australia, and CRC for Molecular Engineering & Technology, CSIRO, North Ryde NSW 2113, Australia

Received November 21, 1994; Revised Manuscript Received February 21, 1995⊗

ABSTRACT: Leucine zippers constitute a widely observed structural motif which serves to promote both homo- and heterodimerization in a number of DNA-binding proteins. As part of our ongoing efforts to characterize both the structure and the dynamical properties of this dimerization domain as they relate to biological function, we report here the secondary structure in solution of a recombinant dimeric peptide (rJunLZ) comprising residues Arg276-Asn314 of the leucine zipper domain of c-Jun. Two- and three-dimensional homo- and heteronuclear NMR experiments have allowed definition of the secondary structure of rJunLZ and have provided a total of ~1500 interproton distance and 62 ϕ dihedral angle constraints for tertiary structure calculations. Amide proton protection factors, calculated from hydrogen−deuterium exchange experiments, have identified 62 hydrogen bonds in the rJunLZ dimer. We have also examined the role of Asn22, the only polar residue situated at the hydrophobic dimer interface. Virtually all leucine zipper sequences contain such a polar residue (usually Asn) near the center of the motif. X-ray crystallographic studies showed that, in the case of the GCN4 homodimer, the polar residue (Asn) adopts an asymmetric conformation in an otherwise essentially symmetric structure. In contrast, all NMR studies of leucine zipper homodimers to date have suggested that the dimers are completely symmetric in solution. We present evidence that the side-chain amide protons of Asn22 are hydrogen-bonded in solution and that this side chain exchanges rapidly between two distinct conformations. On the basis of these observations, we propose a dynamic model which can explain the apparent differences in symmetry observed in NMR and X-ray crystallographic studies of leucine zipper homodimers. We show that mutation of Asn22 to a hydrophobic Leu residue markedly increases the thermal stability of the rJunLZ homodimer, consistent with a destabilizing role for this residue. However, at temperatures below 30 °C, the Asn22 → Leu mutant rearranges to form oligomers larger than the dimer, as was previously observed for the corresponding Asn → Val mutation in the GCN4 leucine zipper. These results are consistent with the hypothesis that the polar Asn residue commonly observed at the interface of leucine zippers imposes specificity for the dimer structure at the expense of stability [Harbury, P. B., Zhang, T., Kim, P. S., & Alber, T. (1993) *Science 262*, 1401−1407].

The leucine zipper is a protein dimerization motif found in two classes of DNA-binding transcription factors; the basic-domain-leucine zipper proteins (bZIP) and the basic-helix-loop-helix-leucine zipper proteins (bHLH-ZIP). Although their DNA-binding motifs differ, the leucine zipper domains are required in both cases for DNA binding. The leucine zipper mediates the precise dimerization required to bring two DNA-binding domains into appropriate juxtaposition to bind transcription enhancer sequences. This requirement for dimerization is related to the dyad symmetry of the cognate enhancer sequences: each half of the dimer occupies one half-site on the DNA (Hurst, 1994). This dependence on dimerization means that DNA binding is regulated not only by the interactions of the DNA-binding domains with DNA but also by the strength of the interaction between the leucine zipper domains (Alber, 1992).

Dimerization of leucine zipper proteins occurs via the formation of a short parallel coiled coil of α-helices. The leucine zipper is characterized by a heptad repeat of leucine residues (Landschulz *et al.*, 1988), and following conventional nomenclature for leucine zipper heptad repeats [(abcdefg)$_n$] (Hurst, 1994), the leucine residues are found at position d (Figure 1). Another heptad repeat of hydrophobic residues, usually comprising the β-branched residues Ile, Thr, or Val, is found at position a. The coiled coil is formed by residues at the a and d positions from two monomers packing against one another to create a hydrophobic interface, conforming to Crick's "knobs-into-holes" model (Crick, 1952), with each residue at positions a and d being surrounded by four others from the neighboring helix. The coiled coil is further stabilized by polar groups in the positions adjacent to the hydrophobic interface (e and g) forming interhelical ion pairs. These polar residues also contribute to the stability of the hydrophobic interface via the packing of their methylene groups against the residues in the a and d positions (O'Shea *et al.*, 1991). Thus the leucine zipper coiled coil is stabilized by a delicate balance of hydrophobic and electrostatic interactions (O'Shea *et al.*, 1992; Thompson *et al.*, 1993).

† This work was supported by research grants to G.F.K. and A.S.W. from the National Health and Medical Research Council of Australia and the University of Sydney Cancer Research Fund.

* Address correspondence to this author.
‡ University of Sydney.
§ CSIRO.

⊗ Abstract published in *Advance ACS Abstracts,* April 1, 1995.

0006-2960/95/0434-6164$09.00/0

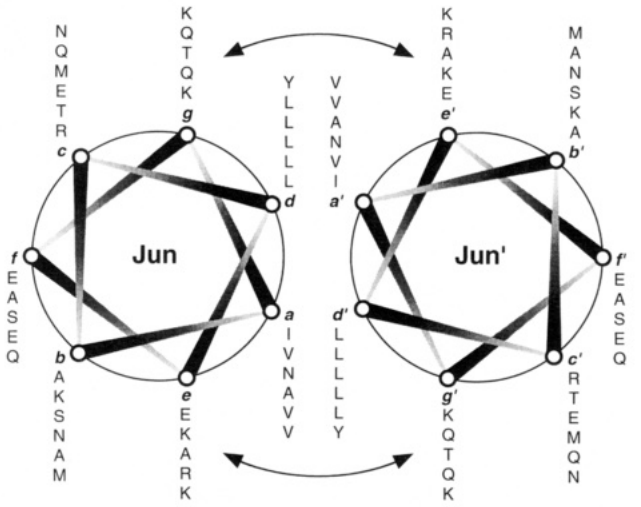

FIGURE 1: Helical wheel representation of residues 8−46 of the rJunLZ homodimer, highlighting the predominance of nonpolar residues found at the dimer interface (positions a and d). Arrows indicate interactions between residues at positions e and g that further stabilize dimer formation via a combination of hydrophobic and electrostatic interactions.

An ususual feature of leucine zippers is the presence of a polar residue (usually Asn) at the a position within the hydrophobic interface, which generally occurs in the middle of the leucine zipper domain (Hurst, 1994). X-ray crystallographic studies of GCN4 (O'Shea *et al.*, 1991) have shown that this a-position Asn residue adopts an asymmetric conformation in the crystal and that it packs more loosely against adjacent residues than do other a-position residues. Substitution of this Asn by a Val dramatically stabilizes the GCN4 coiled coil (Alber, 1992). Thus it would appear that the Asn residue acts as a destabilizing element for the leucine zipper dimer. It has been suggested that this destabilization may help to make dimerization reversible (O'Shea *et al.*, 1991), thereby facilitating the reassociation of monomers into different arrays of homodimers and heterodimers in order to modulate the range of genes affected (McKnight, 1991).

Toward our aim of obtaining a high-resolution solution structure of the Jun leucine zipper, we have applied multidimensional $^1H-^{15}N$ heteronuclear NMR techniques to a 5.1-kDa peptide fragment of c-Jun (rJunLZ; Riley *et al.*, 1994) which encompasses the leucine zipper motif and exists in solution as a disulfide-linked 10.2-kDa dimer. Preliminary analysis of both two- and three-dimensional NMR experiments indicates that rJunLZ forms an almost completely symmetric coiled-coil dimer of parallel α-helical strands which is very similar, if not identical, to the structure we reported previously for a 43-residue synthetic peptide (sJunLZ; Junius *et al.*, 1993) which encompasses the same region of c-Jun. These experiments have also revealed that the conserved polar residue at position a (Asn22) displays different NMR properties to the other two Asn residues found in rJunLZ. These differences suggest that the side-chain amide protons of Asn22 participate in the formation of hydrogen bonds and that this bonding arrangement is dynamic. We present a model of Asn side-chain "flipping" which can rationalize the difference in symmetry observed in the crystal and solution structures of GCN4.

MATERIALS AND METHODS

Materials. Sodium 3-trimethylsilyl[2,2,3,3-$^2H_4$]propionate (d_4-TSP)[1] was obtained from Fluka AG (Buchs, Switzerland), while D_2O (99.96% isotopic purity) and trifluoroacetic acid (TFA) were from Sigma Chemical Co. (St. Louis, MO). All other chemicals were analytical grade.

Computers and Computer Programs. The program UXNMR (SGI version 940501.2), used for fast Fourier transformation of NMR spectra, was obtained from Bruker Australia Pty Ltd (Sydney). The programs EASY (Eccles *et al.*, 1991) and XEASY (Xia and Bartels, unpublished), used for spectral analysis, peak assignment, and peak integration, were kindly provided by Professor Kurt Wüthrich (ETH, Zürich). All spectral transformations, analyses, and cross-peak integrations were performed on either a SUN SPARCstation 2GX or Silicon Graphics Indigo R4000 computer. Nonlinear least-squares curve fitting was carried out using either Regression M1.23 (Blackwell Scientific Publications, U.K.) or KaleidaGraph 2.1.1 (Abelbeck Software) running on an Apple Macintosh personal computer.

Protein Expression. Production of rJunLZ from a bacterial expression system has been described previously (Riley *et al.*, 1994); briefly, the protein is expressed using a pJLZ plasmid obtained by cloning a synthetic *junLZ* gene into the pGEX-2T expression vector (Smith & Johnson, 1988). rJunLZ differs slightly from a synthetic peptide, first described by O'Shea *et al.* (1989), which was used in our previous NMR studies (sJunLZ; Junius *et al.*, 1993); the recombinant peptide has a Gly-Ser-Met extension at the N-terminus and, unlike sJunLZ, is not N-terminally acetylated. An Asn22 → Leu mutation was introduced into pJLZ using the Transformer site-directed mutagenesis kit (Clontech), which is based on the method of Deng and Nickoloff (1992). The unique *Pst*I restriction site in the pJLZ plasmid was removed during the mutation procedure using a selection primer, thus allowing selection of candidate mutant clones by *Pst*I restriction digestion. The final clone was confirmed by DNA sequencing, and the mutant rJunLZ peptide was overexpressed and purified as described previously (Riley *et al.*, 1994).

NMR Experiments. Heteronuclear NMR experiments were performed on a sample containing 2.8 mg of uniformly ^{15}N-labeled rJunLZ dimer dissolved in a solution composed of 450 μL of H_2O, 50 μL of D_2O, 5 μL of 10 mM d_4-TSP (in H_2O), and 5 μL of 100 mM NaN_3 (in H_2O), pH 3.6. The final dimer concentration was 0.54 mM (*i.e.*, 1.1 mM rJunLZ monomer). All NMR experiments were recorded on a Bruker AMX-600 spectrometer equipped with a B-VT 2000 temperature regulation unit. Unless otherwise stated, experiments were acquired at 37 °C. For experiments performed at temperatures below 37 °C, a Bruker B-CU 05 cooling unit was employed to precool the input air supplied to the probe head to approximately −40 °C. Spectra were recorded with either an inverse broadband or proton-observe triple resonance probe head tuned to the frequencies of ^1H and ^{15}N. The ^1H-frequency scale of all spectra was directly

[1] Abbreviations: 2D, two-dimensional; 3D, three-dimensional; d_4-TSP, sodium 3-trimethylsilyl[2,2,3,3-$^2H_4$]propionate; HMQC, heteronuclear multiple quantum coherence; HSQC, heteronuclear single quantum coherence; NMR, nuclear magnetic resonance; ppm, parts per million; NOESY, nuclear Overhauser enhancement spectroscopy; rf, radio frequency; TFA, trifluoroacetic acid.

referenced to d_4-TSP at 0.00 ppm, while the ^{15}N-frequency scale was indirectly referenced to liquid NH_3 using the method of Live *et al.* (1984).

NOESY Experiments. The 3D $^1H-^{15}N$ NOESY-HMQC spectrum (mixing time = 100 ms) was acquired at a spectral size of 512 × 48 × 128 ($t_3 \times t_2 \times t_1$) data points using the pulse sequence described by Fairbrother *et al.* (1991), except that the two spin-lock pulses (used for water suppression) were implemented using the same rf field strength as for hard pulses. The data was linear-predicted (up to 768 points in t_3, 64 points in t_2, and 192 points in t_1), treated with identical weighting functions in each frequency dimension (a squared sine bell shifted by $\pi/3$), and Fourier-transformed to give a final data matrix of 1024 × 64 × 256 ($F_3 \times F_2 \times F_1$) real data points. For comparison, a 2D $^1H-^1H$ NOESY spectrum was acquired using the same sample and mixing time. The effects of $^{15}N-^1H$ *J*-couplings were negated by the application of a π (^{15}N) refocusing pulse during the ^1H evolution time and GARP decoupling during the acquisition period. Prior to Fourier transformation, the raw data matrix of 2048 × 512 ($t_2 \times t_1$) complex data points was zero-filled once in each dimension and treated with a Lorentz–Gauss function in t_2 and a $\pi/3$-shifted sine bell squared function in t_1.

$^3J_{HN\alpha}$ Coupling Constants. The backbone $^3J_{HN\alpha}$ coupling constants of rJunLZ were measured using the technique described by Billeter *et al.* (1992) in which a series of 2D $^1H-^{15}N$ *J*-modulated heteronuclear single quantum coherence (HSQC-*J*) spectra are recorded. A delay (τ_2), which precedes the final ^1H observe pulse, is systematically varied across the series, resulting in a modulation of cross-peak intensity according to the magnitude of the $^3J_{HN\alpha}$ coupling involving each amide proton. The nature of this modulation is described by

$$\bar{V}(\tau_2) = A[\cos(\pi J\tau_1)\cos(\pi J\tau_2) - 0.5\sin(\pi J\tau_1)\sin(\pi J\tau_2)]e^{-\tau_2/T_2'} \quad (1)$$

where $\bar{V}$ is the cross-peak volume as a function of the delay time τ_2, A is the cross-peak volume at $\tau_2 = 0$, J is the $^3J_{HN\alpha}$ coupling constant, and T_2' is the apparent transverse relaxation time.

For each experiment, 2048 complex points were recorded in t_2 with a spectral width of 5747 Hz and with the ^1H carrier placed on the H_2O signal. 128 increments were collected in t_1, with a spectral width of 1200 Hz. The H_2O signal was suppressed using low-power presaturation during the intertransient delay, together with a 2-ms spin-lock purge pulse (Messerle *et al.*, 1989). Nine separate experiments were acquired using τ_2 values of 10, 20, 35, 50, 65, 80, 95, 110, and 125 ms. The nine sets of data were each linear-predicted up to 200 points in t_1, treated with identical weighting functions (Lorentz-Gauss in t_2 and a squared sine bell shifted by $\pi/2$ in t_1), and transformed using the same phase corrections to give a final data matrix of 2048 (F_2) × 512 (F_1) real data points. A polynomial baseline correction was applied to the processed spectra in F_2. Cross-peak volumes were measured using XEASY. The data for each residue were fitted to eq 1 by using an in-house implementation of the Simplex nonlinear least-squares algorithm (Press *et al.*, 1989) to minimize the function

$$\chi^2 = \sum_{i=1}^{n}[V(\tau_2^i) - \bar{V}(\tau_2^i)] \quad (2)$$

where $V(\tau_2^i)$ is the experimental cross-peak intensity, and $\bar{V}(\tau_2^i)$ is the cross-peak intensity calculated from eq 1 during the curve-fitting process. This fitting procedure gives optimized values of $^3J_{HN\alpha}$, A, and T_2'. Errors in the derived values of $^3J_{HN\alpha}$ were estimated using the method described by Billeter *et al.* (1992) whereby, for each residue, A and T_2' were optimized for a range of fixed values of $^3J_{HN\alpha}$. The upper and lower error bounds for $^3J_{HN\alpha}$ were taken to be the values for which $\chi^2 = 2\chi^2_{min}$.

Amide Proton Exchange Rates. Amide proton exchange rates were measured by recording a series of 2D $^1H-^{15}N$ HSQC experiments (Bax *et al.*, 1990; Norwood *et al.*, 1990) following dissolution of the fully protonated ^{15}N-labeled rJunLZ sample in D_2O. The zero time for the experiment was recorded when D_2O, precooled to 4 °C, was added to the sample tube containing lyophilized rJunLZ, also at 4 °C. The sample was then transferred to the probe, which had been preequilibrated at 37 °C. The acquisition of the first experiment began within 8 min of sample dissolution. A total of 28 experiments was recorded, each with 100 t_1 increments of 2048 complex data points, using the same acquisition parameters described previously (Riley *et al.*, 1994). The number of scans per t_1 increment was varied according to the following scheme to maximize the number of time points sampled at the beginning of the time course and then to maximize the signal-to-noise ratio at the end: experiments 1–4, 8 scans; 5–8, 16 scans; 9–15, 32 scans; 16–22, 48 scans; and 23–28, 64 scans. The data were appropriately scaled prior to Fourier transformation to account for the differing number of scans. Spectral resolution in both dimensions was enhanced by apodization with a squared sine bell function shifted by $\pi/2$ and the digital resolution of the spectra was improved by zero-filling to 2048 × 512 ($F_2 \times F_1$) real data points. Following phase correction, all spectra were baseline-corrected using third-order polynomials.

Peak intensities were measured by volume integration of a set of rectangular regions manually fitted to the peaks using the EASY program (Eccles *et al.*, 1991). The exchange rate constant (k_{ex}) for each amide proton was obtained by fitting plots of cross-peak intensity (I) versus time (t) to the following function:

$$I = I_0 e^{-k_{ex}t} + I_\infty \quad (3)$$

where I_0 and I_∞ are the cross-peak intensities at zero and infinite time, respectively. Theoretical random coil exchange rates of the backbone amide protons of rJunLZ at pH 3.6 were calculated using eq 2 of Bai *et al.* (1993). The acid, base, and water reference rate constants used for the calculation were taken from Table 3 of Bai *et al.* (1993) for a blocked alanine tripeptide and were modified by the application of eq 3 of Bai *et al.* (1993) to give rates for 37 °C. The protection factors (P) against amide proton exchange, imposed by the structure of rJunLZ, were calculated by dividing the theoretical random coil rates by the observed rates. The protection factor for the side-chain amide group of Asn22 was calculated in a similar fashion but using the reference rates for dipeptides, listed in Table 4 of Bai *et al.* (1993).

Temperature Dependence of Amide Proton Cross-Peak Intensity. The effect of temperature on amide proton cross-peak intensity was monitored by recording a series of five $^1H-^{15}N$ HSQC spectra at 0, 5, 10, 20, and 30 °C. The sample was preequilibrated for 30 min at each temperature, and 80 dummy scans were employed at the start of each experiment to ensure that any increase in sample temperature due to the application of ^{15}N decoupling pulses had stabilized prior to acquisition of data. Each experiment consisted of 128 t_1 increments of 2048 complex data points; other acquisition and processing parameters were as described previously (Riley *et al.*, 1994).

Circular Dichroic Spectroscopy. CD experiments were performed using a Jasco-720 spectropolarimeter interfaced to an Osborne personal computer for automatic data collection. Wavelength scans (182−260 nm) were performed at discrete temperatures from 4 to 95 °C using peptide concentrations of ~15 μM in a 1-mm cylindrical quartz cell. Sample pH was 3.6 as for the NMR studies. Temperature was maintained using a Neslab circulating water bath connected to a water-jacketed cell holder. Each spectrum was the sum of four scans; data points were collected at 0.5-nm intervals using a scan rate of 20 nm min^{-1}, a time constant of 1 s, and a bandwidth of 1 nm. Buffer blanks, run under identical conditions, were subtracted from the data. Spectral signal-to-noise was optimized by multiplying the frequency power spectrum by a trapezoidal apodization function prior to Fourier transformation.

Thermal unfolding transitions were monitored by measuring the ellipticity at 222 nm (θ_{222}) as a function of temperature. Transition temperature(s), T_m, were estimated from the θ_{222} versus temperature data by evaluating the maximum of $d\theta/dT$.

HPLC Studies of Mutant rJunLZ. rJunLZ (Asn22 → Leu) was injected onto a reverse-phase C18 column (Applied Biosystems Inc.; 10 × 1 cm, 20-μm particle size) and eluted at a flow rate of 4.0 ml min^{-1} using a linear gradient of 50% solvent A (0.1% TFA in water)/50% solvent B (0.1% TFA in acetonitrile) to 100% solvent B over 30 min. Peptide elution was detected by simultaneously monitoring the absorbance at 215 and 276 nm using an LKB 2141 variable-wavelength detector.

RESULTS

Identification of Secondary Structure. The secondary structure of rJunLZ was ascertained by examination of the 3D NOESY-HMQC spectrum. Although the overlap observed in 2D NOESY spectra of sJunLZ is not prohibitive of structure calculation, there are some regions which lead to high levels of ambiguity, such as shown in Figure 2A. In contrast, the extra resolution offered by the 3D NOESY-HMQC (cf. Figure 2A with Figure 2B−F) enabled most of the ambiguities observed in the 2D NOESY to be resolved. As was observed in the 2D spectra of the sJunLZ peptide (Junius *et al.*, 1993), only one complete set of resonances corresponding to the primary structure of the monomer could be seen in the 3D NOESY-HMQC spectrum, suggesting that the rJunLZ dimer is completely symmetric. Thus the analysis of secondary structure was limited to NOE cross peaks previously shown by O'Donoghue *et al.* (1993) to result solely or predominantly from intramonomer dipolar connectivities.

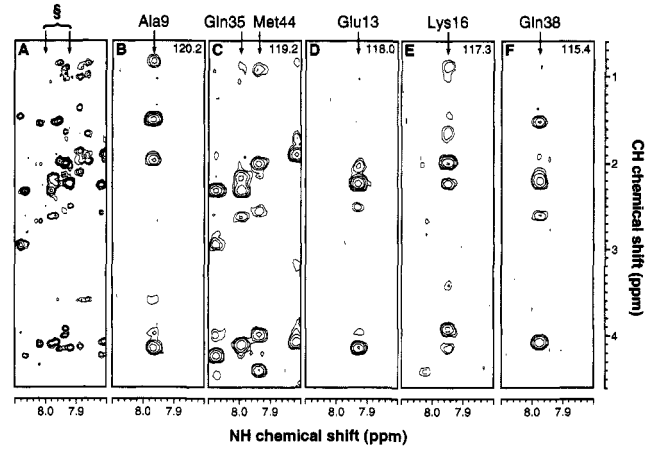

FIGURE 2: Comparison of spectral resolution obtained in 2D and 3D NOESY experiments on ^{15}N-labeled rJunLZ dimer. (A) Portion of the amide-aliphatic region of the 2D $^1H-^1H$ NOESY of rJunLZ. The frequencies bracketed by arrows (§) contain resonances from six backbone amide protons. (B−F) Slices of the corresponding $\omega_1-\omega_3$ planes in the 3D $^1H-^{15}N$ NOESY-HMQC spectrum of rJunLZ showing how all of the six backbone amide proton resonances are unambiguously resolved. The ^{15}N chemical shift of each plane (in parts per million) is given at the top of each spectrum.

Assignments of ^{15}N, αCH, and NH chemical shifts were made on the basis of those already reported for rJunLZ (Riley *et al.*, 1994). Comparison of rJunLZ and sJunLZ αCH chemical shifts (Junius *et al.*, 1993; Riley *et al.*, 1994) revealed a small number of minor differences. This was assumed to hold true for the βCH protons, the assignments of which were based upon the chemical shifts of those observed for sJunLZ at the same pH and temperature.

Figure 3 summarizes the structurally important intramonomer connectivities observed for rJunLZ. Like the synthetic sJunLZ dimer, rJunLZ displays a large number of $d_{NN}(i, i+1)$ connectivities along the whole length of the peptide. These NOEs, along with the presence of many $d_{\alpha N}(i, i+3)$, $d_{\alpha N}(i, i+4)$, and $d_{\alpha\beta}(i, i+3)$ connectivities, strongly suggest that rJunLZ forms an extended α-helix in the same manner as sJunLZ.

$^3J_{HN\alpha}$ Coupling Constants. The $^3J_{HN\alpha}$ coupling constants for 43 of the 45 backbone ϕ angles were determined using the HSQC-*J* procedure of Billeter *et al.* (1992) as described under Materials and Methods. These values are listed in Table 1, together with their upper and lower error bounds, and the calculated values of A and T_2'. Figure 4A shows fits of eq 1 to the experimental data for four different residues. The fits were generally very good.

The dependence of the quality of the curve fit on the value of $^3J_{HN\alpha}$ is illustrated in Figure 4B for the same four residues. The minimum of each curve represents the optimized coupling constant obtained when J, A, and T_2' from eq 1 are all fitted simultaneously, and the gradient of the curve on either side of the minimum indicates how well A and T_2' can be fitted to other values of $^3J_{HN\alpha}$ when the latter is fixed in the calculation. Thus, steep gradients, such as are observed for Gln45, imply very small error ranges for the measured coupling constant, while shallower gradients correspond to larger errors. The curves shown in Figure 4B are representative of the range seen over the entire peptide, with lower limits generally less well defined than upper ones.

Figure 4C shows the values of the error ranges obtained for coupling constants of different sizes. Residues with

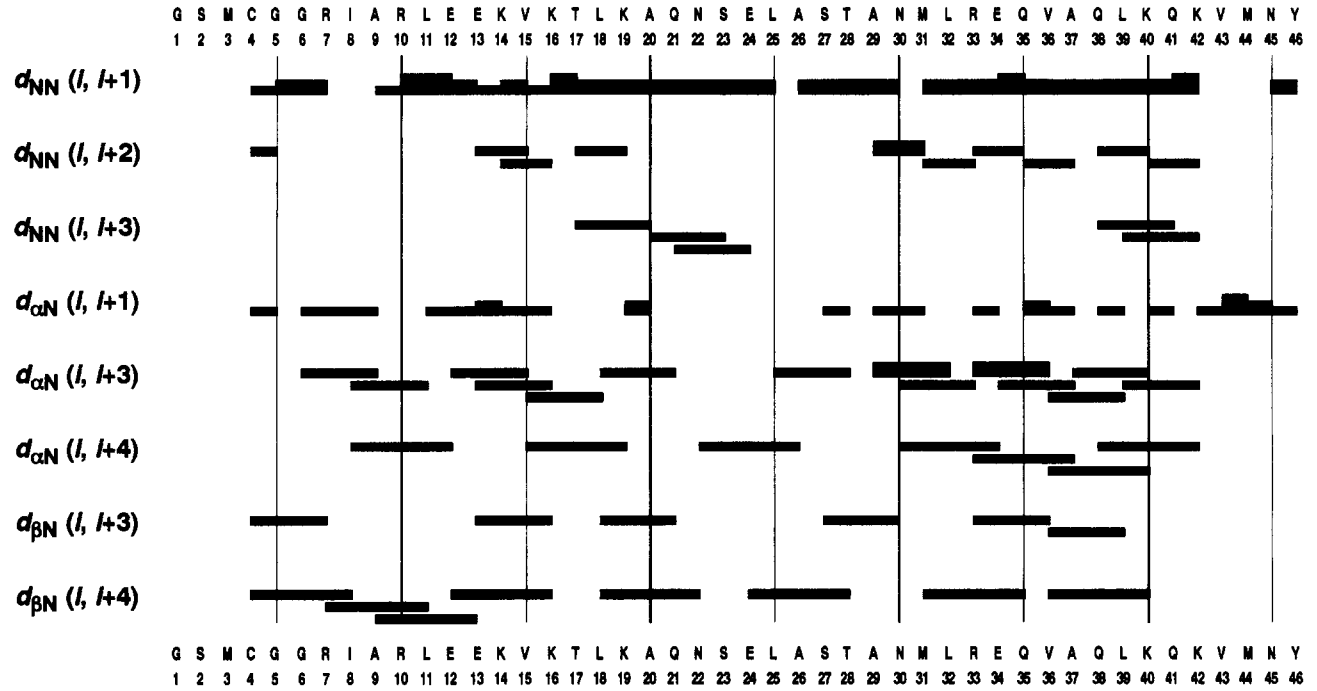

FIGURE 3: Summary of the structurally important intramonomer NOESY connectivities observed for the rJunLZ dimer. The NOE cross-peak intensities observed in the 3D $^1H-^{15}N$ NOESY-HMQC were classified into three categories by counting contour levels and are represented in the graphs by the height of the bars.

smaller coupling constants display larger error ranges, as noted previously by Billeter *et al.* (1992). Note, however, that this lack of lower-limit precision does not compromise the usefulness of the derived coupling constants, as the structure calculations for which they will be used only take into account whether or not the measured coupling constant is <5 Hz, which thereby determines a range of allowed values for the associated dihedral angle.

The $^3J_{HN\alpha}$ coupling constants are clearly consistent with the published helical structure of the JunLZ monomer (Junius *et al.*, 1993), which was derived primarily from NOE constraints, and will serve as valuable additional constraints in the structure calculations currently being carried out on the JunLZ dimer.

Amide Proton Exchange Rates. Examples of the $^1H-^{15}N$ HSQC spectra used to measure the amide proton exchange rates are shown in Figure 5. The first HSQC spectrum acquired during the amide exchange time course (Figure 5A) comprises resonances from the backbone amide protons of residues 11−41 inclusive and the resonances of the side-chain amide group of Asn22. The side-chain protons, and most of the backbone amide protons, are still not exchanged for deuterons after 95 min (Figure 5B). After 2128 min (Figure 5C), only 12 of the backbone resonances remain, half of which belong to interfacial residues. For all of these residues, except Gln41, a plot of peak intensity versus time is well-fitted by an exponential decay; examples of these fits are shown in Figure 5D. Although the Gln41 backbone NH group was visible in the early spectra from the time course, it was not possible to reliably fit an exponential function to the measured intensities due to the rapid decay of this peak.

Structural protection factors (*P*) were calculated for the backbone amide protons of residues 11−40 and for the side-chain amide protons of Asn22. The fastest exchange rate calculated was 2.21 ± 0.14 s^{-1}, which provides a lower limit for the exchange rates of the remaining residues, and for the corresponding protection factors. The protection factors for residues 11−40 (Table 2) range from 86 to 5060 and do not show any appreciable correlation with the primary structure (Figure 6A). However, close examination of the *P* values reveals a correlation with position within the heptad repeat (Figure 6B), as was observed previously for the GCN4 leucine zipper (Goodman & Kim, 1991). The residues at the a and d positions, within the dimer interface, are on average more protected than those at other positions, while those residues at position c are consistently less protected. The size of the *P* values does not appear to correlate with the hydrogen-bond lengths predicted from amide proton chemical shifts [see Figure 6 of Junius *et al.* (1993)] but instead is more dependent upon whether or not the amide group is located within the dimer interface; this conflicts with the good correlation between *P* values and hydrogen-bond lengths observed for the GCN4 leucine zipper (Goodman & Kim, 1991). Calculation of the average *P* values for each position within the heptad repeat reveals that the dimer interface provides a 2−6-fold increase in protection against exchange when compared to all other positions except c. The reason for residues in the c position being less protected than other noninterfacial residues (especially f) is not clear; however, the GCN4 leucine zipper displays a similar pattern of amide proton exchange (Goodman & Kim, 1991).

Calculation of *P* for the Asn22 γNH_2 protons shows that their exchange rates are slowed approximately 4400-fold by comparison to the expected rate in an unstructured dipeptide. This level of protection is comparable to the *P* values seen for the backbone amide protons located at the dimer interface (positions a and d). Taking account of the 2−6-fold increase in *P* attributable to positioning of the residue at the dimer interface, the Asn22 γNH_2 still shows *P* values of about 1000, suggesting that they are involved in the formation of one or more hydrogen bonds. Note that there is no

Table 1: $^3J_{HN\alpha}$ Coupling Constants and Other Parameters Derived from Equations 1 and 2 for rJunLZ at 37 °C[a]

residue	$^3J_{HN\alpha}$ (Hz)	J_l[b] (Hz)	J_u[b] (Hz)	A[c]	T_2' (ms)
Ser2	6.7	5.6	7.9	3.9	61
Met3	5.7	5.5	5.9	1.3	63
Cys4	6.6	5.2	7.8	0.7	40
Arg7	4.4	3.0	4.9	5.1	39
Ile8	5.0	0.0	6.3	3.9	28
Ala9	2.2	0.0	3.4	5.0	36
Arg10	4.8	4.2	5.2	6.6	42
Leu11	5.4	3.8	6.2	4.8	34
Glu12	0.0	0.0	5.9	0.9	32
Glu13	4.6	3.7	5.2	4.9	40
Lys14	4.3	3.1	4.9	5.7	32
Val15	3.4	1.9	4.2	3.4	37
Lys16	3.2	2.0	3.9	5.2	37
Thr17	4.9	3.4	5.7	3.3	39
Leu18	4.6	0.0	5.8	2.2	30
Lys19	3.8	0.0	5.7	0.9	36
Ala20	4.7	4.4	4.9	6.1	42
Gln21	4.4	3.7	4.9	3.6	41
Asn22	3.9	0.0	5.0	1.1	42
Ser23	3.7	2.0	4.5	3.6	39
Glu24	4.7	4.1	5.1	5.4	40
Leu25	4.2	1.6	5.2	1.4	34
Ala26	4.1	0.0	5.2	1.4	42
Ser27	4.4	3.7	4.8	4.5	43
Thr28	3.6	0.0	4.8	2.2	35
Ala29	3.6	0.0	5.3	1.9	38
Asn30	3.7	2.4	4.4	4.4	43
Met31	4.7	3.8	5.3	4.7	36
Leu32	4.1	0.0	5.5	2.5	32
Arg33	2.1	0.0	5.1	2.1	33
Glu34	5.0	4.5	5.3	6.5	40
Gln35	4.5	3.8	4.9	5.2	37
Val36	0.0	0.0	3.6	2.6	26
Ala37	2.7	0.0	3.7	6.5	38
Gln38	4.9	4.5	5.2	5.0	42
Leu39	4.3	2.3	5.2	3.1	33
Lys40	1.9	0.0	5.0	2.4	31
Gln41	5.5	5.2	5.8	8.3	46
Lys42	6.5	6.2	6.7	7.3	47
Val43	6.9	6.6	7.2	7.3	47
Met44	6.8	6.6	7.0	7.0	64
Asn45	8.0	7.9	8.1	6.7	94
Tyr46	7.4	7.3	7.5	10.0	75

[a] The three glycine residues (Gly1, Gly5, and Gly6) are omitted. [b] The upper and lower error limits for $^3J_{HN\alpha}$ (J_u and J_l, respectively), obtained from the grid search described in Materials and Methods, are the values of $^3J_{HN\alpha}$ for which $\chi_2 = 2\chi^2_{min}$. [c] Cross-peak volume at τ_2 = 0 (see Materials and Methods).

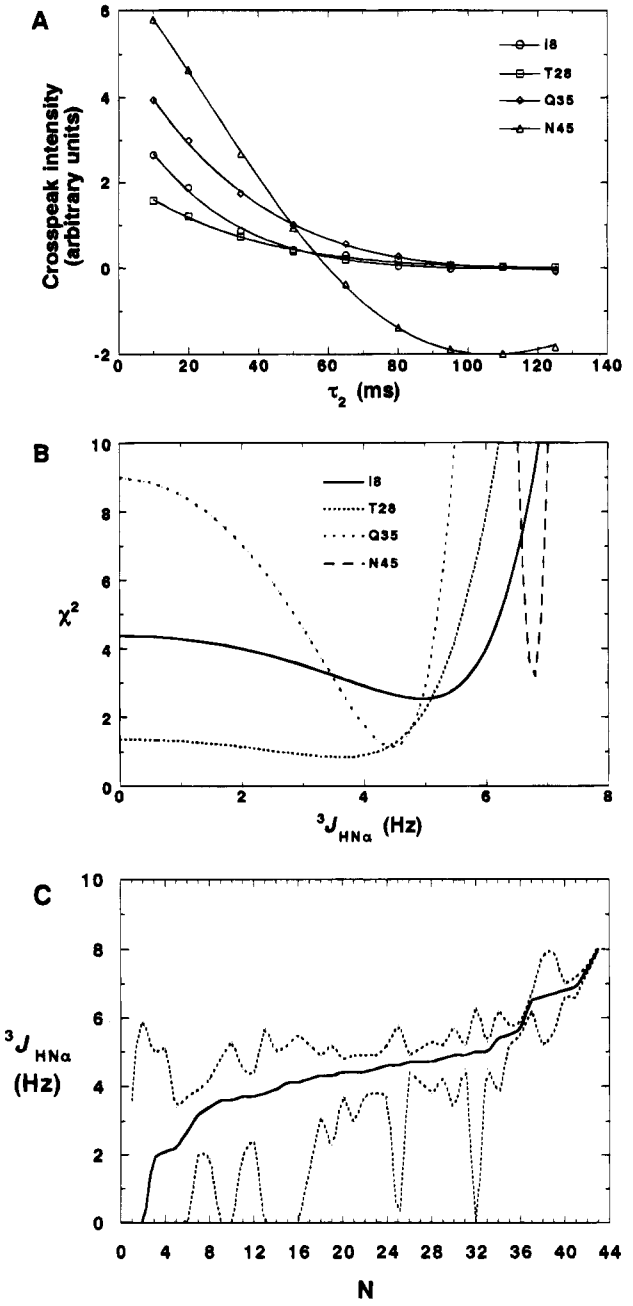

FIGURE 4: (A) Plot of cross-peak volume versus τ_2 for residues Ile8 (○, $^3J_{HN\alpha}$ = 5.0 Hz), Thr28 (□, $^3J_{HN\alpha}$ = 3.6 Hz), Gln 35 (◇, $^3J_{HN\alpha}$ = 4.5 Hz), and Asn45 (△, $^3J_{HN\alpha}$ = 8.0 Hz) of rJunLZ, illustrating the influence of $^3J_{HN\alpha}$ on the nature of the volume dependence. These plots represent typical fits of the experimental data to eq 1. (B) Plot of the goodness-of-fit parameter, χ^2, against $^3J_{HN\alpha}$ for the same residues shown in panel A. The poor definition of the lower error limit can be seen for residues Ile8 and Thr28 in particular. (C) Plot of the coupling constant $^3J_{HN\alpha}$ (solid line) and the calculated error ranges (dotted line) for rJunLZ. Note that the ordering of the abscissa is by coupling-constant size rather than residue number. The trend of poorly defined lower limits for smaller values of $^3J_{HN\alpha}$ is clear.

appreciable difference in the P values of the two protons of the Asn22 γNH_2 group, indicating that both protons must be involved in hydrogen bonds (although not necessarily simultaneously).

Effect of Temperature on Amide Proton Cross-Peak Intensity. In an HSQC experiment recorded at 30 °C, the intensities of the Asn22 γNH_2 signals are somewhat lower than those of the other amide side-chain protons in the peptide (see Figure 7A). Lowering the sample temperature reduces the intensities of the Asn22 γNH_2 signals (while leaving the other Asn and Gln amide proton intensities unaffected), and at 0 °C they are indistinguishable from the baseline noise (Figure 7B–E). This loss of intensity could result from line broadening due to either chemical exchange or restricted motion leading to fast T_2 relaxation. The fact that the loss of intensity with temperature is completely selective for the Asn22 γNH_2 signals, and is not seen for any other interfacial residue, strongly argues that the broadening is not a result of severely restricted motion. Rather, this loss of intensity must be attributable to some chemical exchange process which moves from the "fast exchange" regime at room temperature towards the "intermediate exchange" regime at temperatures <5 °C. In other words, the Asn22 side chain exists in solution in two (or more) distinct conformations, which interconvert sufficiently rapidly at room temperature to give rise to an NMR signal

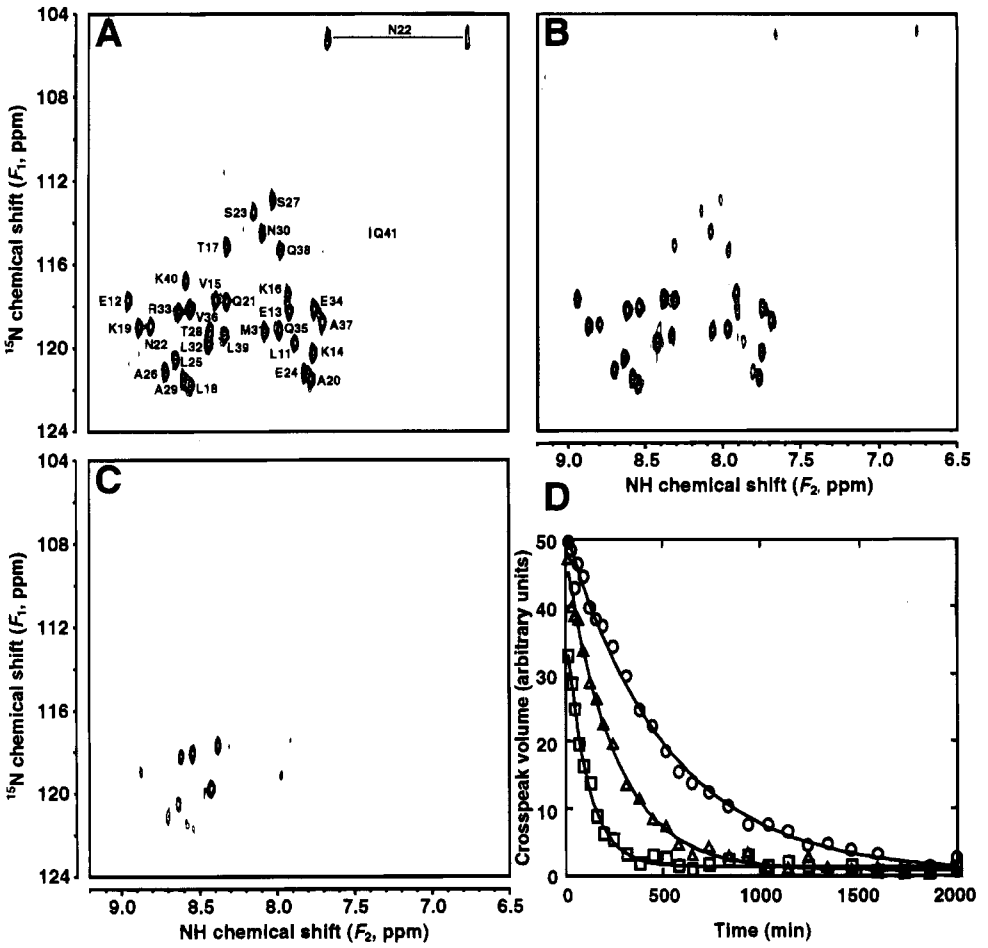

FIGURE 5: Time course of proton-deuteron exchange in ^{15}N-labeled rJunLZ. ^{1}H−^{15}N HSQC spectra recorded (A) 17 min, (B) 95 min, and (C) 2128 min after dissolution of rJunLZ in D_2O. (D) Decay of peak intensities with time for the backbone amide protons of Val15 (○), Asn22 (□), and Gln35 (△). The curves correspond to those obtained from fitting eq 3 to the data.

which is averaged on both the ^{1}H and ^{15}N chemical shift time scales. Unfortunately, it was not possible to follow the transition through to the "slow exchange" regime in order to observe the side-chain cross peaks corresponding to each of the distinct conformations accessed by the Asn22 γNH_2 protons.

Thermal Denaturation of Native rJunLZ Peptide and Asn22 → Leu Mutant. A series of CD spectra acquired at various temperatures during thermal denaturation of the disulfide-bonded rJunLZ dimer is shown in Figure 8A. The CD spectrum changes from one characteristic of an α-helical conformation at low temperature (*i.e.*, negative minima at 208.5 and 222 nm and a positive maximum at 191.5 nm), to one characteristic of random coil at high temperature (*i.e.*, a negative minimum at 201 nm and a positive maximum at 187.5 nm). The well-defined isodichroic point at 203.1 nm is consistent with a transition from folded dimer to unfolded "monomer" without significant population of intermediate states. In other words, the leucine zipper helices are only stable when in the coiled-coil conformation, as previously noted for GCN4 (Thompson *et al.*, 1993).

The progressive melting of the rJunLZ dimer was monitored by following the ellipticity at 222 nm (θ_{222}) as a function of temperature; this curve (Figure 8B) reveals that the unfolding process is highly cooperative, with a transition temperature, T_m, of 52 °C.

An overlay of a series of CD spectra acquired at various temperatures during thermal denaturation of the Asn22 → Leu mutant dimer (see Figure 8C) reveals the absence of an isodichroic point, consistent with a more complicated unfolding transition than the two-state process observed for the native rJunLZ dimer. Indeed, the melting curve obtained for the Asn22 → Leu mutant (see Figure 8D) reveals two unfolding transitions at 20 and 75 °C. The second transition (T_m = 75 °C) is concentration-independent (data not shown) and therefore corresponds to melting of the disulfide-linked dimer. The first transition is concentration-dependent (data not shown), indicating that the mutant dimer self-associates at low temperature. Thus, the low T_m corresponds to unfolding of this oligomer to give the dimer.

We have not investigated the nature of this oligomer in detail, but HPLC studies of the mutant peptide are consistent with the CD results. Incubation of the peptide for 15 min at 37 °C leads to a single HPLC peak at $R_T \sim 22$ min (lower trace, Figure 8E), corresponding to the disulfide-linked dimer, while incubation at 20 °C leads to the appearance of an additional peak at $R_T \sim 18.5$ min (lower trace, Figure 8E), corresponding to the oligomer. The reduced retention time for this species on a reverse-phase HPLC column is consistent with a switch from a two-stranded to a four-stranded coiled coil, since X-ray crystallographic studies of native and mutant GCN4 leucine zippers have revealed that the hydrophobic interfacial residues are more buried in tetrameric as compared to dimeric coiled coils (Harbury *et al.*, 1993). However, the evidence obtained thus far does not preclude the presence of higher-order oligomers.

Table 2: List of Exchange Rates and Calculated P Values for the Amide Protons of rJunLZ

residue	k_{ex} (s^{-1})	protection factor (P)
Gly1	>2.21	<12500
Ser2	>2.21	<186
Met3	>2.21	<1070
Cys4	>2.21	<308
Gly5	>2.21	<847
Gly6	>2.21	<229
Arg7	>2.21	<36
Ile8	>2.21	<214
Ala9	>2.21	<91
Arg10	>2.21	<34
Leu11	1.08 ± 0.07	756 ± 50
Glu12	0.28 ± 0.01	1080 ± 30
Glu13	0.78 ± 0.03	814 ± 32
Lys14	0.48 ± 0.02	287 ± 10
Val15	0.12 ± 0.01	2950 ± 130
Lys16	0.29 ± 0.01	595 ± 18
Thr17	1.15 ± 0.05	86 ± 4
Leu18	0.25 ± 0.01	1620 ± 90
Lys19	0.29 ± 0.01	263 ± 11
Ala20	0.39 ± 0.01	1090 ± 40
Gln21	0.32 ± 0.01	2740 ± 100
Asn22	0.57 ± 0.02	1850 ± 80
Ser23	1.48 ± 0.08	700 ± 40
Glu24	1.04 ± 0.05	144 ± 7
Leu25	0.14 ± 0.00	5060 ± 150
Ala26	0.18 ± 0.01	2250 ± 100
Ser27	1.45 ± 0.07	166 ± 8
Thr28	1.23 ± 0.08	459 ± 31
Ala29	0.29 ± 0.01	4860 ± 190
Asn30	0.79 ± 0.03	352 ± 12
Met31	0.63 ± 0.04	248 ± 15
Leu32	0.09 ± 0.00	4680 ± 200
Arg33	0.14 ± 0.00	2120 ± 60
Glu34	0.52 ± 0.02	1050 ± 50
Gln35	0.24 ± 0.01	579 ± 19
Val36	0.10 ± 0.01	4690 ± 280
Ala37	0.31 ± 0.01	759 ± 20
Gln38	0.87 ± 0.03	88 ± 3
Leu39	0.53 ± 0.02	768 ± 25
Lys40	2.21 ± 0.14	91 ± 6
Gln41	>2.21	<154
Lys42	>2.21	<41
Val43	>2.21	<165
Met44	>2.21	<287
Asn45	>2.21	<89
Tyr46	>2.21	<23
Asn22 Nγ1[a]	1.6 ± 0.1	4290 ± 240
Asn22 Nγ2[a]	1.5 ± 0.1	4540 ± 250

[a] The Asn22 side chain amide proton exchange rates were limited to one decimal place by the reference rates given in Bai *et al.* (1993).

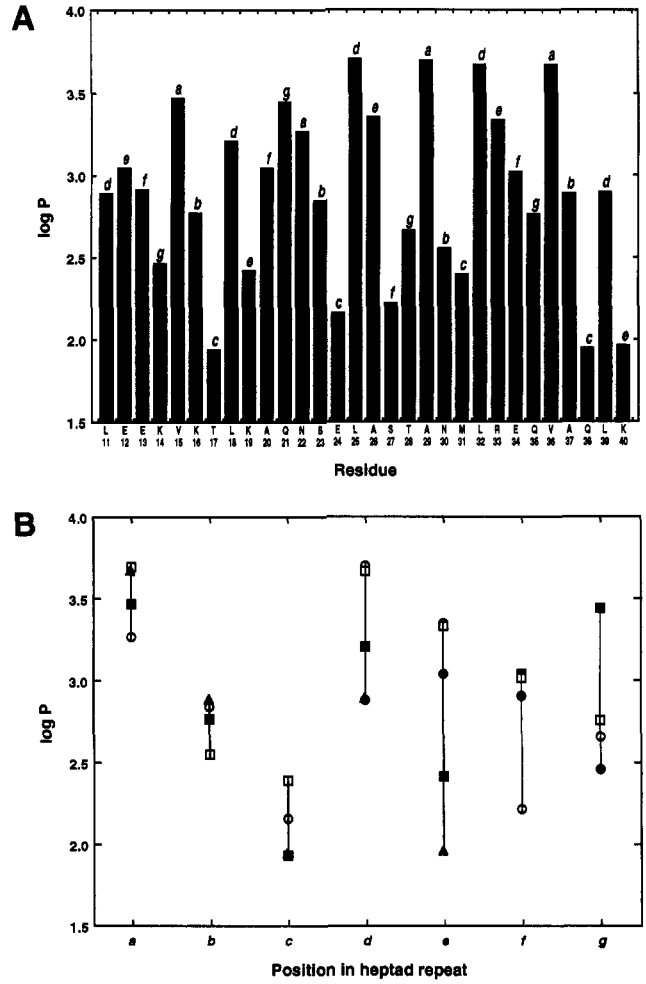

FIGURE 6: Protection of backbone amide protons from exchange with solvent deuterons. (A) Log of the protection factors plotted as a function of residue. (B) The same data ordered by residue position (a–g) within each heptad repeat (●, residues 11–14; ■, residues 15–21; ○, residues 22–28; □, residues 29–35; ▲, residues 36–40).

DISCUSSION

In this paper we have presented the results of $^{1}H-^{15}N$ heteronuclear NMR experiments performed on the rJunLZ peptide. These experiments suggest that rJunLZ forms a symmetric dimer comprising a coiled coil of two α-helices. Thus it would appear that rJunLZ forms a structure very similar, if not identical, to that previously reported for sJunLZ (Junius *et al.*, 1993).

The use of ^{15}N labeling has permitted us to examine more closely the amide groups within the leucine zipper domain of Jun, and we have shown that the side-chain amide protons of Asn22 behave differently than those of Asn30 and Asn45. First, the Asn22 γNH_2 cross peaks are shifted 5 ppm to low frequency in the ^{15}N dimension relative to the frequencies of the Asn30 and Asn45 γNH_2 cross peaks [see Table 1 of Riley *et al.* (1994)], which is consistent with their being located in the different chemical environment of the hydrophobic interface.

Second, and perhaps more striking, is the reduced exchange rate of the Asn22 γNH_2 group. The two factors contributing to this protection from exchange are (i) burial from solvent, due to the amide group being located at the hydrophobic interface, and (ii) hydrogen bonding. The contribution of burial from solvent to the overall protection factor can be clearly seen in the larger protection factors observed for backbone amide protons at positions a and d, which lie at the dimer interface (Figure 6B). However, given that hydrogen bonding is the major determinant of slow exchange (Englander & Kallenbach, 1984), it is almost certain that the side chains of both Asn22 residues in the dimer are involved in one or more hydrogen bonds. This is supported by the observation of an apparent hydrogen bond between the side chains of the conserved a-position Asn residues (Asn264) in crystal structures of the isolated GCN4 leucine zipper (O'Shea *et al.*, 1991) and in complexes of the GCN4 bZIP domain with both the AP-1 (Ellenberger *et al.*, 1992) and ATF/CREB (Konig & Richmond, 1993) DNA regulatory elements.

Examination of the tertiary structure of the sJunLZ dimer (Junius, O'Donoghue, Mackay, Weiss, and King, unpub-

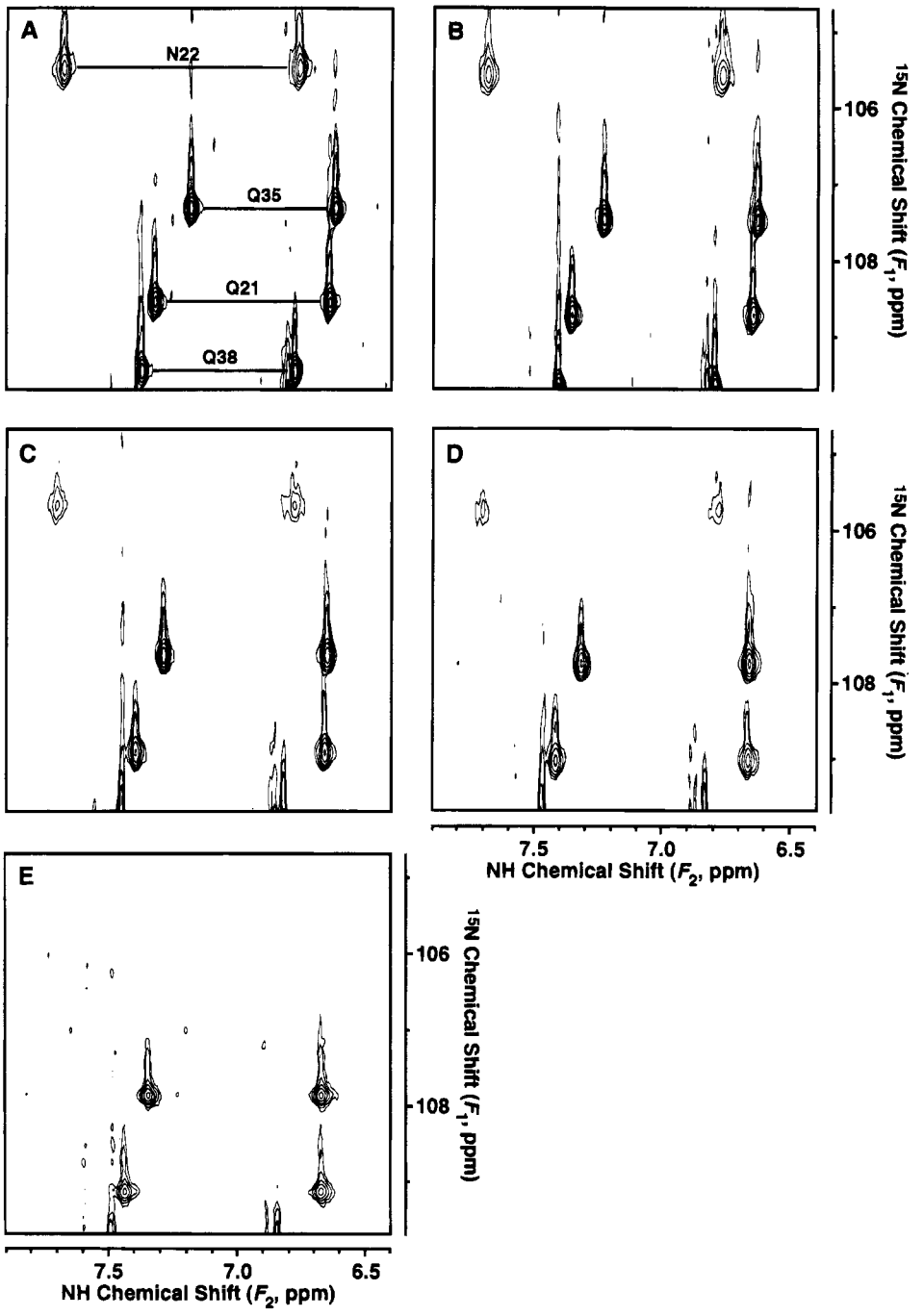

FIGURE 7: Variation of amide proton cross-peak intensity with temperature in rJunLZ. The same region of $^{15}N-^{1}H$ HSQC spectra recorded at various temperatures showing the γNH_2 resonances arising from Asn22, Gln35, Gln21, and Gln38: (A) 30 °C, (B) 20 °C, (C) 10 °C, (D) 5 °C, and (E) 0 °C. The upfield lobes on each cross peak in the ^{15}N dimension are the result of the deuterium isotope effect in the 10% of NHD moieties present in the solution (Bax *et al.*, 1990). Note the disappearance of the Asn22 cross peaks at 0 °C. The Gln38 cross peaks shift downfield in the ^{15}N dimension during the temperature titration.

lished data) reveals that, just like Asn16 in GCN4, the most feasible way of forming a hydrogen bond is by pairing the amide protons of one Asn22 side chain to the carbonyl oxygen of the Asn22 residue in the neighboring monomer. However, the asymmetric hydrogen-bonding arrangement seen in the GCN4 crystal structure (O'Shea *et al.*, 1991) would lead to a different chemical environment for each Asn residue, which could potentially manifest itself as separate NMR resonances for each Asn side chain. No such asymmetry has been reported in any of the NMR studies on the GCN4 dimer (Oas *et al.*, 1990; Saudek *et al.*, 1990), nor is it apparent in the spectra reported here for rJunLZ. There are two possible explanations which can reconcile this discrepancy: either the Asn side chains pack in a symmetrical conformation in solution, or they exchange between asymmetric conformations at a rate sufficiently rapid to give rise to a single, population-weighted average chemical shift (O'Shea *et al.*, 1991). The results of the low-temperature HSQC experiments reported here, which show that Asn22 is involved in a conformational exchange process, strongly support the latter explanation.

On the basis of these results we have devised a model (see Figure 9A) in which the side chains of both Asn residues undergo rapid 180° reorientations around the $\beta C-\gamma C$ bond, which allow each side chain to "flip" between two distinct conformations: either the Asn22 γNH_2 is close to, and

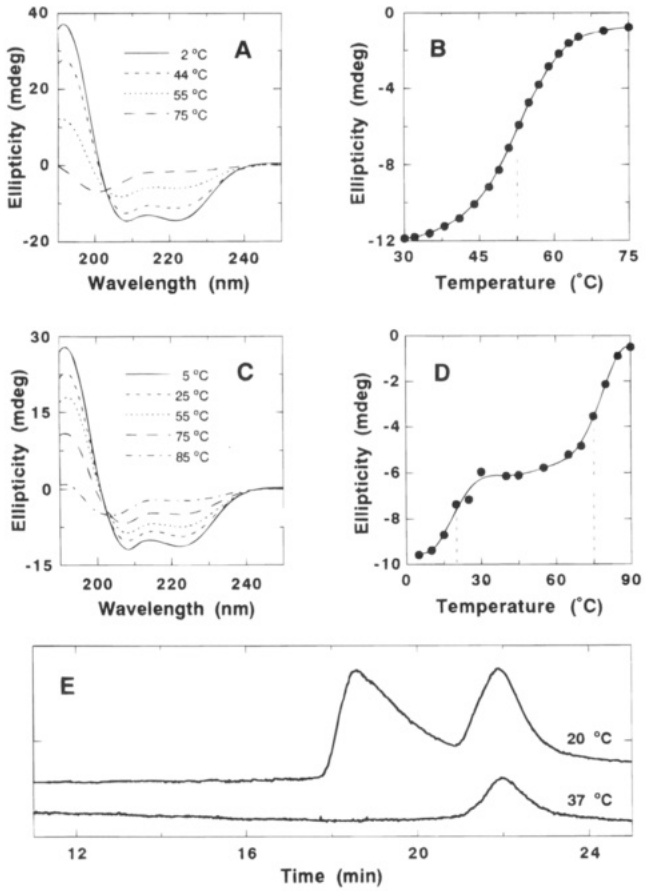

FIGURE 8: Thermal denaturation of rJunLZ. (A) Far-UV CD spectra recorded at various temperatures during the thermal denaturation of rJunLZ; note the isodichroic point at 203.1 nm. (B) Thermal denaturation curve for rJunLZ; a plot of $d\theta/dT$ reveals a T_m of 52 °C. (C) Far-UV CD spectra recorded at various temperatures during the thermal denaturation of the rJunLZ(Asn22 → Leu) mutant. (D) Thermal denaturation curve for rJunLZ(Asn22 → Leu); a plot of $d\theta/dT$ reveals two unfolding transitions at 20 and 75 °C. (E) Reverse-phase HPLC chromatograms of rJunLZ-(Asn22 → Leu) following incubation of the peptide for 15 min at temperatures of 37 °C (lower trace) and 20 °C (upper trace). At both of these temperatures, native rJunLZ elutes as a single species with $R_T \sim 16.5$ min.

H-bonds with, the Asn22′ γCO or the Asn22′ γNH_2 is close to, and H-bonds with, the Asn22 γCO. In addition, the identity of the H−D exchange rates for the two protons of the γNH_2 group suggests that either (i) both protons are simultaneously H-bonded to the carbonyl oxygen of the other Asn residue (*i.e.*, a bifurcated H-bond, as shown in Figure 9A), or (ii) only one of these two protons is H-bonded at a given instant, and they are interchanged by a 180° rotation about the γN−γC bond. We cannot at present distinguish between these two possibilities. Note that an alternative, symmetric arrangement, in which both γNH_2 groups are simultaneously involved in intermonomer H-bonds (Figure 9B), may be discounted. In this model the side-chain amide protons of the two Asn residues are always in equivalent environments (because the structure is symmetric), and this is inconsistent with the NMR temperature titration, which indicates that these amide groups interconvert between *two distinct conformations*.

Note that although the conformation of each of the two Asn22 side chains is altered in the exchange process shown in Figure 9A, *the global structure of each of these two dimers is completely identical (and asymmetric overall).* Thus when

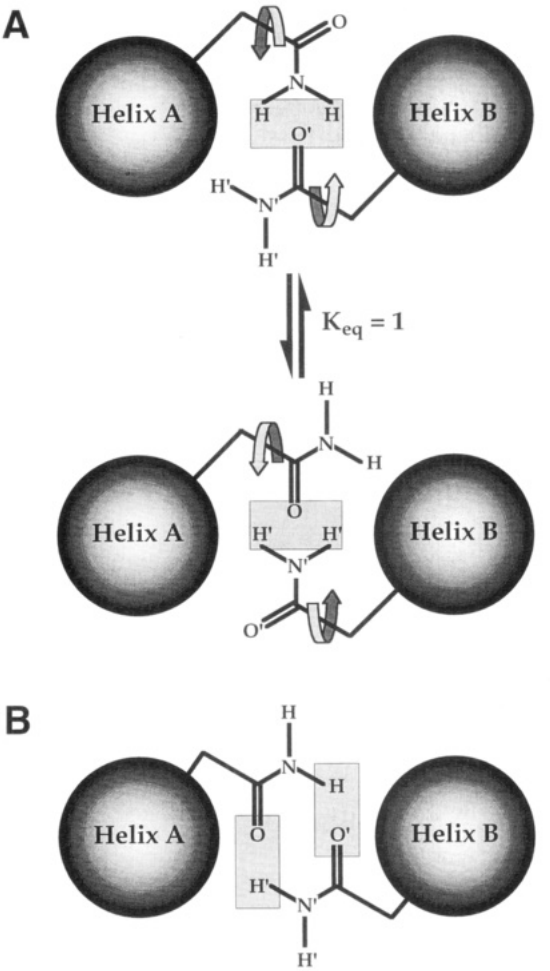

FIGURE 9: (A) Asymmetric model for Asn22 side-chain hydrogen bonding. The two dimers shown interconvert through concerted 180° rotations about the two βC−γC bonds (see arrows). Note that these two dimers are in fact *chemically identical* and can be superimposed by rotating either one through 180° about an axis normal to the page. In addition, the hydrogen-bonding arrangement (shaded boxes) may be bifurcated as shown or may involve only a single amide proton with rotation around the γC−γN bond leading to each proton being H-bonded for equivalent time periods. This model is consistent with all NMR and X-ray diffraction data collected on leucine zippers to date. (B) Symmetric model for Asn22 side-chain hydrogen bonding. This model is inconsistent with the variable-temperature HSQC data, which implicate a chemical exchange process involving these side-chain amide protons.

this structural motif is viewed using a relatively static technique such as X-ray crystallography (as for the GCN4 dimer; O'Shea *et al.*, 1991), the asymmetry of the side-chain arrangement is apparent, while the dynamic exchange process occurring in solution may be overlooked. This serves as an important reminder of the complementarity of X-ray crystallographic and solution-state NMR techniques. Note also that the crystal structure of GCN4 shows additional asymmetry at Lys15 and Glu20 (O'Shea *et al.*, 1991). Given that these two residues are outside the dimer interface and exposed to solvent, it is highly probably that their side chains are in constant motion in the solution state. Thus, it seems likely that the asymmetry seen for these residues is a direct consequence of crystal packing. This is supported by the observation that Lys15 makes an intermolecular contact via a water molecule.

The model of Asn side-chain flipping that we have proposed is consistent with the suggestion that this residue

acts as a destabilizing agent (O'Shea *et al.*, 1991; Alber, 1992), thus facilitating the rapid reassortment of monomer pairs and altering the range of homo- and heterodimeric bZIP and bHLH-ZIP transcription factors which can activate genes in response to extracellular growth signals. In order to test this hypothesis, we mutated the Asn22 residue in rJunLZ to a leucine residue which we would expect to be more stable in the hydrophobic milieu of the coiled-coil interface, especially since this mutation would presumably preclude the conformational exchange process observed for Asn22. As expected, the Asn22 → Leu mutant had a thermal unfolding transition which was 23 °C higher than that observed for the native rJunLZ peptide (compare Figure 8, panels B and D). Somewhat surprisingly, however, the Asn22 → Leu mutant was found to polymerize beyond the dimer at low temperature. A similar result was observed when the corresponding Asn residue in the GCN4 leucine zipper was mutated to a Val residue (Harbury *et al.*, 1993). Thus, our results confirm the suggestion made by Alber, Kim, and colleagues (Harbury *et al.*, 1993) that the polar Asn residue commonly observed at the interface of leucine zippers imposes specificity for the dimer structure at the expense of stability.

All studies of leucine zippers to date have centered on homodimers, yet proteins like Fos require heterodimerization for activity. Of particular interest is to probe the behavior of the Jun Asn22 residue when located within the Jun/Fos heterodimer, where it must interact with a Lys residue in the Fos leucine zipper. Although the major determinant of the instability of the Fos homodimer appears to be the large number of acidic residues occupying positions e and g (O'Shea *et al.*, 1992), (see Figure 1), it is possible that the a-position Lys residues in Fos (of which there are two) also make a destabilizing contribution. Studies of the structural properties of the Jun-Fos heterodimer in solution using multidimensional homo- and heteronuclear NMR techniques are currently in progress in this laboratory. In addition, we are currently using heteronuclear (^{15}N) relaxation measurements on both the Jun−Jun homodimer and the Jun−Fos heterodimer to assess whether interfacial polar residues cause deformations which manifest as altered dynamical properties.

ACKNOWLEDGMENT

This work was conducted as part of the Australian Commonwealth Government's Cooperative Research Centre for Molecular Engineering and Technology: Sensing and Diagnostic Technologies. We thank Ms. Lisa Riley and Ms. Natalie Wieland for preparation of the ^{15}N-labeled rJunLZ.

REFERENCES

Alber, T. (1992) *Curr. Opin. Genet. Dev. 2*, 205−210.
Bai, Y., Milne, J. S., Mayne, L., & Englander, S. W. (1992) *Proteins: Struct., Funct., Genet. 17*, 75−86.
Bax, A., Ikura, M., Kay, L. E., Torchia, D. A, & Tschudin, R. (1990) *J. Magn. Reson. 86*, 304−318.
Billeter, M., Neri, D., Otting, G., Qian, Y. Q., & Wüthrich, K. (1992) *J. Biomol. NMR 2*, 257−274.
Crick, F. H. C. (1952) *Nature 170*, 882−883.
Deng, W. P., & Nickoloff, J. A. (1992) *Anal. Biochem. 200*, 81−88.
Eccles, C., Güntert, P., Billeter, M., & Wüthrich, K. (1991) *J. Biomol. NMR 1*, 111−130.
Ellenberger, T. E, Brandl, C. J., Struhl, K., & Harrison, S. C. (1992) *Cell 71*, 1223−1237.
Englander, S. W., & Kallenbach, N. R. (1984) *Q. Rev. Biophys. 16*, 521−655.
Fairbrother, W. J., Cavanagh, J., Dyson, J. H., Palmer, A. G., III, Sutrina, S. L., Reizer, J., Saier, M. H., Jr., & Wright, P. E. (1991) *Biochemistry 30*, 6896−6907.
Goodman, E. M., & Kim, P. S. (1991) *Biochemistry 30*, 11615−11620.
Harbury, P. B., Zhang, T., Kim, P. S., & Alber, T. (1993) *Science 262*, 1401−1407.
Hurst, H. (1994) *Protein Profile 1*, 123−152.
Junius, F. K., Weiss, A. S., & King, G. F. (1993) *Eur. J. Biochem. 214*, 415−424.
König, P., & Richmond, T. J. (1993) *J. Mol. Biol. 233*, 139−154.
Landschulz, W. H., Johnson, P. F., & McKnight, S. L. (1988) *Science 240*, 1759−1764.
Live, D. H., Davis, D. G., Agosta, W. C., & Cowburn, D. (1984) *J. Am. Chem. Soc. 106*, 1939−1941.
McKnight, S. L. (1991) *Sci. Am. 264*, 32−39.
Messerle, B. A., Wider, G., Otting, G., Weber, C., & Wüthrich, K. (1989) *J. Magn. Reson. 85*, 608−613.
Norwood, T. J., Boyd, J., Heritage, J. E., Soffe, N., & Campbell, I. D. (1990) *J. Magn. Reson. 87*, 488−501.
Oas, T. G., McIntosh, L. P., O'Shea, E. K., Dahlquist, F. W., & Kim, P. S. (1990) *Biochemistry 29*, 2891−2894.
O'Donoghue, S. I., Junius, F. K., & King, G. F. (1993) *Protein Eng. 6*, 557−564.
O'Shea, E. K., Rutkowski, R., Stafford, W. F., III, & Kim, P. S. (1989) *Science 245*, 646−648.
O'Shea, E. K., Klemm, J. D., Kim, P. S., & Alber, T. (1991) *Science 254*, 539−544.
O'Shea, E. K., Rutkowski, R., & Kim, P. S. (1992) *Cell 68*, 699−708.
Press, W. H., Flannery, B. P., Teukolsky, S. A., & Vetterling, W. T. (1989) *Numerical recipes in Pascal: the art of scientific computing*, Cambridge University Press, Cambridge, England.
Riley, L. G., Junius, F. K., Swanton, M. S., Vesper, N. A., Williams, N. K., King, G. F., & Weiss, A. S. (1994) *Eur. J. Biochem. 219*, 877−886.
Saudek, V., Pastore, A., Castiglione Morelli, M. A., Frank, R., Gausepohl, H., Gibson, T., Weih, F., & Rosch, P. (1990) *Protein Eng. 4*, 3−10.
Smith, D. B., & Johnson, K. S. (1988) *Gene 67*, 31−40.
Thompson, K. S., Vinson, C. R., & Freire, E. (1993) *Biochemistry 32*, 5491−5496.

BI942694S